Characterizing A549 NSCLC Microtissue Model Toward Functional Precision Medicine

By

Daniel Chait

Biochemistry B.A. University of South Florida, 2023

Thesis

Submitted in partial fulfillment of the requirements for the Degree of Master of Science in the Graduate Program of Biotechnology at Brown University

PROVIDENCE, RHODE ISLAND

May 2025

AUTHORIZATION TO LEND AND REPRODUCE THE THESIS

As the sole author of this thesis, I authorize Brown University to lend it to other institutions for the purpose of scholarly research.

Date_____ _____

Daniel Chait, Author

I further authorize Brown University to reproduce this thesis by photocopying or other means, in total or in part, at the request of other institutions or individuals for the purpose of scholarly research.

Date_____ _____

Daniel Chait, Author

This thesis by Daniel Chait is accepted in its present form by the Graduate Program in Biotechnology as satisfying the thesis requirements for the degree of Master of Science

Date_____ Signature: _____

Dr Jonghwan Lee, Advisor

Date_____ Signature: _____

Dr. Jeffrey Morgan, Reader

Date_____ Signature: _____

Dr. Diane Hoffman-Kim, Reader

Approved by the Graduate Council

Date_____ Signature: _____

Dr. Thomas Lewis, Dean of the Graduate School

Acknowledgments

I am incredibly thankful to Dr. Jonghwan Lee for this fantastic opportunity, for allowing me to pursue my research interest, and for giving me tremendous support, insight, and advice when preparing and delivering my research. I would also like to thank Ahbid Zein-Sabatto not only as PhD graduate in the lab but also as a mentor in the intricacies of graduate-level research. Thank you for guiding me throughout my entire time being a part of this lab. I also want to thank my fellow committee members, Dr. Jeffrey Morgan and Dr. Diane Hoffman-Kim; I appreciate the support you two have shown and the advice you have given me. Lastly, I would like to thank every member of the Lee lab for helping me prepare for my thesis presentation and providing insight on how to present my data better.

I am highly appreciative of all the opportunities bestowed upon me by being able to attend Brown University. Specifically, Dr. Jacquelyn Schell and the rest of the biotechnology master's program administrators, staff, faculty, and students have all positively impacted me, and I am thankful to you all.

Finally, I want to thank the tremendous external support from friends and family over the previous two years. If it were not for your continued support behind the scenes, I don't know if I would be here today finishing this degree. I am beyond grateful to have you all in my life.

Table of Contents

Table of Figures

Table of Tables

Abstract

Objective: Lung cancer is the top cause of cancer-related deaths, expected to claim 227,000 lives by 2025. It has two main subtypes: Non-Small Cell Lung Cancer (NSCLC), which comprises 85% of cases, and Small Cell Lung Cancer (SCLC). Major issues include delays in diagnosis and treatment. A personalized treatment strategy, particularly through Functional Precision Medicine (FPM), is essential, focusing on heterogeneity and sample size limitations. Strategies like spheroid cultures and Optical Coherence Tomography (OCT) can address these challenges. **Methods:** Aim 1: focuses on optimizing the spheroid development of A549 by comparing different growth media (DMEM, RPMI, and F12k) and seeding densities (50 x 10^3, 100 x 10^3, 200 x 10^3, and 400 x 10^3) to achieve optimal cell growth. For Aim 2: utilizing the best spheroid development from Aim 1, a drug testing experiment was conducted with drugs (Cisplatin, Sotorasib, and Afatinib) across dosage ranges of (0 μM, 0.7 μM, 7 μM, and 35 μM). **Results**: Aim 1: A549 spheroid development optimization revealed through morphological images, ATP analysis, and Live/Dead analysis that the most optimal growth media and seeding density were RPMI at a seeding density of 50k. Aim 2: The drug testing comparison study presented unexpected results. Afatinib was the only drug to show a significant effect through ATP analysis, while Cisplatin and Sotorasib demonstrated no statistically significant effects. **Conclusion:** In conclusion, optimal A549 spheroid development using microtissue models was successful. Further testing for drug studies is necessary due to inconclusive ATP data. Future OCT viability assessments for drug testing A549 spheroids will occur.

Keywords: Lung Cancer, NSCLC, A549, 3D Cell Culture, FPM, ATP, Live/Dead, Drug Testing

Chapter 1: Introduction

1.1: The Societal Effects of Lung Cancer

Lung cancer is at the forefront of cancer-related deaths across the entire globe. Having two variations, lung cancer can be identified as either Non-Small Cell Lung Cancer (NSCLC) or Small Cell Lung Cancer (SCLC). The American Cancer Society estimates that there will be approximately 227,000 new lung cancer cases in 2025, with an estimated death toll of 125,000. [1,2]. NSCLC makes up approximately 85% of all lung cancer-related cases, while SCLC accounts for the other 15%. NSCLC can be subjected to three subtypes: adenocarcinoma, squamous cell carcinoma, and large cell carcinoma. Adenocarcinomas grow on the outer parts of the lung and are the most common subtype for all NSCLC cases, making up 40% [3-6]. Squamous cell carcinomas typically grow more slowly and generally arise in one of the bronchi of the lungs. In contrast, the rarest subtype, large cell carcinoma, proliferates more rapidly and often metastasizes more easily. The most significant challenge associated with NCLC stems from its lethality, with an average 5-year survival rate of 28% for all stages combined [1,2]. Many complications arise from delays attributed to the patient's diagnosis and treatment [7,8].

1.2: A Personalized Method to Medicine

A more personalized approach might be most beneficial to both patients and physicians when overcoming issues of treatment ineffectiveness. This customized approach to medical treatment is also called precision medicine, which refrains from focusing on an “ideal average patient” with a “one size fits all” mindset. Instead, it evaluates patients as individuals with their unique genetic makeup. There are many factors to consider when creating a personalized therapeutic guide for patients. The most common approach is evaluating the genetic profiling of patients, also known as genome precision medicine. Genomic profiling within the field of

oncology has led to tremendous breakthroughs. The study by Yang et al. identified many germline and somatic variants that play vital roles in cancer progression and classifies many unique structural variations and copy number variations that also affect cancer progression [9]. Genome precision medicine has many benefits, but it has its limitations. It does not consistently predict tumor response to drugs, and the presence of heterogeneity can lead to chemoresistance, hindering prolonged survival rates and accurate drug resistance predictions. [10]. The solution to these limitations is to take a more functional precision medicine approach to oncology.

1.3: A Functional Approach to Personalized Medicine

Functional precision medicine (FPM) takes patient-derived tumor cells and screens them using various drugs. Observing the biopsied tumor response creates a personalized therapeutic guide for each patient. The variations within and among numerous tumor cells make it insufficient to depend exclusively on genomic profiling. Even though some patients benefit from this approach, more information regarding tumor cell vulnerability can be discovered through FPM [11]. Practical challenges must be overcome to use FPM in a clinical environment. Culturing the cells in a proliferative microenvironment comparable to in vivo is crucial when using biopsied tumor cells. Switching from 2D cell culture to 3D/spheroid cell culture techniques may address these challenges since 3D models better mimic the cells' complex biological processes, such as cell-to-cell and cell-to-matrix interactions [12-15]. Incorporating these physiologically relevant factors in the model helps maintain its clinical relevance and ability to predict drug response, which is crucial for the success of FPM.

1.4: Optical Coherence Tomography

Another substantial variable that must be addressed is the limited sample size. Testing drug effectiveness immediately and over time is crucial for a patient's well-being. A non-

invasive, label-free assay capable of longitudinally evaluating 3D cell viability is essential. The proposed solution is Optical Coherence Tomography (OCT), a non-invasive imaging technique that uses light waves to capture cross-sectional images. Initially utilized for retina imaging, it shows potential for capturing images of 3D tissue growth while detecting intracellular motion, motility, and viability [16-18]. Compared to other viability imaging methods, OCT does not utilize fluorescent dyes or reagents, which often have poor diffusion and may negatively influence the samples, leading to skewed results. The contrast in OCT arises from the backscattered light due to differences in refractive indices, providing a label-free contrast compared to other fluorescence microscopies [16]. In a study by Jung et al., they demonstrated the use of OCT compared to other established viability assays, such as cytotoxicity. A drug testing experiment was conducted using ovarian cancer spheroid models with PDT, Carboplatin, and their combination. The results indicated that OCT could predict therapeutic efficacy, which cannot be achieved with traditional molecular assays such as Live/Dead [18]. It also correlated apoptosis data with the nodular disruption analysis, providing additional information about the evolution of treatment response. [18]. With further analysis and data collection, OCT could be leveraged to assess the cell viability of various cancer tumor cells, thereby advancing the field of precision medicine.

Chapter 2: Aim 1: Media and Seeding Optimization for A549 Spheroid Development

2.1: Introduction

The A549 non-small cell lung cancer (NSCLC) cell line possesses a well-documented history. Initially identified in 1972 by Giard et al., this line was derived from a biopsy and culture of a cancerous tumor from a 58-year-old Caucasian male [19]. Since its discovery, various oncological biomedical research studies have employed the squamous NSCLC cell line. The experience of the A549 cell line in three-dimensional (3D) cell culture is limited compared to other extensively studied cancer cell lines; therefore, the objective is to optimize the spheroid development of the A549 cancer cells. The effective cultivation of suitable A549 organoid models necessitates the identification of the optimal growth media and seeding density.

Cancer cells require appropriate growth media to proliferate; however, there is currently no procedural standard for 3D A549 cells. The most common media options used or suggested include F12K, DMEM/F12, and RPMI 1640. [20,21]. Moreover, the seeding density for A549 cells must be optimized using the specified 96-well 3D microtissue mold. In a study by Yildiz-Ozturk et al., similar molds were utilized. Their findings indicated excessive seeding density ranges, leading to numerous overgrown spheroid models [21]. As a reference, it was decided to use smaller seeding values and the following seeding densities would be adopted: 50×10^3, 100×10^3, 200×10^3, and 400×10^3. Maximizing the growth potential of the 3D A549 spheroid model is crucial, particularly for the forthcoming Functional Precision Medicine approach to drug development screening.

2.2: Methods & Materials

2.2.1: Cell Culture A549

NSCLC human alveolar epithelial cancer cells (A549; ATCC) were shipped and cultured in Kaighn's Modification of Ham's F-12 Medium (21127022; Gibco^{TM}). Over several weeks, some of the cells were slowly and methodically transitioned into two other recommended media options based on ATCC recommended guidance [22]: Roswell Park Memorial Institute 1640 Medium (A1049101; Gibco^{TM}) and Dulbecco's Modified Eagle Medium F12 (11320033; Gibco^{TM}). All three media options were supplemented with 10% Fetal Bovine Serum (S11150; GeminiBio) and 1% of 10,000 IU/mL penicillin/10,000 µg/ml streptomycin (ICN1670249; Fisher-Scientific), and the cells were incubated at 5% CO_2 at 37 °C.

Prior to transitioning to three-dimensional culture, the cells were cultivated in T-75 flasks (Cell Treat) with 15 mL of the specified media replenished every two to three days. A passage was conducted on day seven, or when the confluence reached 75%. Increments of 2 mL, 2 mL, and 3 mL of 0.25% Trypsin-EDTA (25-200-056; GibcoTM) were administered to detach the cell layer from the flask. The final 3 mL of Trypsin was retained in the flask on the cell layer for seven minutes within the incubator. Subsequently, 12 mL of warm media was introduced into the flask, followed by two rinses of the cell layer, after which the contents of the flask were transferred to a 50 mL tube. The tube underwent centrifugation for six minutes at 125 x g. Excess media and Trypsin were discarded, and the resulting cell pellet was loosened and resuspended in 4 mL of warm media. In a 0.5 mL microcentrifuge tube, 56 µL of 0.4% Trypan Blue (15-250-061; GibcoTM) was mixed with 6 µL of the cell suspension to achieve a 1:10 ratio. Cell counting was performed using 10x magnification with a hemacytometer (02-671-6; Hausser Scientific), applying 10 µL of the trypan/cell mixture on each side. Cell count calculations were

executed to ascertain the requisite cell suspension, which was then transferred to a new T-75 flask containing 15 mL of media. Prior to placement in the incubator, the flask should be gently rocked twenty times, followed by executing four figure-eights to ensure an even distribution of cells throughout the flask. After visually inspecting the flask under the microscope (Leica DMi1 Inverted Phase Contrast Microscope), it was placed in the incubator set at 5% CO2 and 37 °C.

2.2.2: A549 3D Microtissue Formation

Microtissue 3D petri dish micro-mold spheroids (Z764043, Sigma-Aldrich) were formed using a mixture of 100 mL of Phosphate Buffered Saline (10010049, Gibco™) and 2 g of Agarose (16500100; Invitrogen™). Agarose molds were placed individually into a 24-well plate and were equilibrated at least three times with incomplete media before seeding. A549 cells were cultured into the 96-well microtissue molds with complete media. Seeding density varied from 50 $x10^3$, 100 x 10^3, 200 $x10^{3,}$ and 400 x 10^3, accompanied by RPMI, DMEM or F12k for all seeding densities. The spheroids were placed in an incubator for a week, and every two days, morphology images of the spheroids were taken, followed by a media change. Imaging of the cells was conducted using Leica DMi1 Inverted Phase Contrast Microscope on days 2, 4, and 6 in vitro to examine the morphological changes of the spheroids at each seeding density and media option.

The gel seeding procedure is conducted similarly to the passaging procedure mentioned in section 2.2.1. However, the calculations differ slightly during the calculation process. The cell suspension and media volumes must be calculated for the number of gels prepared. Once these calculations are made, the cell suspension and media are mixed. Twenty-five minutes before seeding, the media in the wells should be aspirated and replaced with warm-supplemented media. The wells, including the microtissue wells of the gels, should be aspirated

gently. Once completed, 70 µL of the media/cell suspension mixture will be added to each microtissue mold using a P200 in a dropwise manner to disperse the amount across the entire gel. The gels should sit in the dark for 10 minutes before moving to the incubator for 20 minutes. After 20 minutes, 1 mL of warmed media is added to each well of the 24-well plate, which is then placed back in the incubator at 5% CO2 and 37 °C, with media changes every 2-3 days.

2.2.3: Morphology of A549 Spheroids

Morphology of A549 spheroids was collected on days 4, 5, and 6 in vitro using a Leica DMi1 Inverted Phase Contrast Microscope. Images were taken for each media option (DMEM, RPMI, and F12k) and each seeding density (50 x10^3, 100 x 10^3, 200 x$10^{3,}$ and 400 x 10^3). Approximately 15 spheroids can be captured per image at 10x magnification. When examining the morphology of spheroids, it is essential to consider various phenotypic properties, such as growth rate and overall size, as they provide insight into overall health cells.

2.2.4: CellTiter-Glo Cell Viability Assay

A549 microtissue molds were gently removed from the 24-well plate and placed individually into 35 mm Petri dishes with 3-4 mL of the designated media. Spheroids were extracted by gently flushing media over the gels using a P1000 pipette. Once isolated, a P200 pipette with the tip trimmed to prevent spheroid shearing was used to move a single spheroid along with 90 µL of media to a 96-well plate, and the P200 tip was trimmed to avoid the shearing of the cells. Imaging of the spheroid in each well was conducted using a Leica DMi1 inverted phase contrast microscope to analyze the pixel area of the spheroid, which was utilized for normalization of the ATP results. Using a multi-channel pipet, room-temperature ATP assay reagent (CellTiter-Glo, Promega) was added to each occupied well at 90 µL. Post-treatment of ATP reagent, the 96-well plates were transported to the plate rocker for 5 minutes at 150 RPM;

once completed, the plate was left to sit at room temperature for 25 minutes. Post-rest, the plates were placed into a microplate reader (Synergy HTX, BioTek), measuring the luminescence of the spheroids with ATP reagent.

2.2.5: Live/Dead Viability Assay

A549 gels cultured in RPMI and DMEM at 50k and 100k seeding densities were placed individually into sterile 24-well plates, each receiving 1 mL of warm media mixed with 2 µL/mL of ethidium homodimer and 0.5 µL/mL of Calcein-AM. The samples were incubated at 37 °C with 5% CO_2, shielded from light for 30 minutes. Subsequent gel imaging was performed using a Zeiss Axivert 100 inverted fluorescence microscope at 10x magnification. Twelve tiles were captured and stitched with Zeiss's Zen Pro software, employing Brightfield, EGFP, and Alexa Fluor 568 presets [23]. The microtissues were segmented to ensure a consistent baseline, with adjustments to reduce noise levels.

2.2.6: Statistical Analysis: Spheroid Optimization

CellTiter-Glo Assay was performed by taking eight microtissue replicates per condition for three weeks. A549 cells' ATP data was standardized using the cross-sectional area using the operation, $\frac{ATP}{Pixel\ Area}$. After normalizing the data, a linear Mixed-Effect (LME) model was executed using JMP PRO 17 software (Cary, NC). The LME model considered factors like media and seeding density as full factorials, while the random effect accounted for the variations in passages performed across biological replicates. This analysis allowed for a side-by-side comparison of conditions, facilitating the identification of the most optimal media and seeding density.

Live/Dead assay analysis was conducted by segmenting 20 microtissue spheroids per condition using MATLAB code. Segmentation was done manually, and 10 spheroids were

selected per microtissue mold per condition. The code then extracted various outputs, primarily focusing on intensity fraction and area fraction. The intensity fraction is calculated from the following equation: $IF = \frac{L_I}{L_I + D_I}$. Live intensity was determined by the amount of Calcein in the EGFP channel, while dead intensity was determined by the amount of ethidium homodimer present in the Alexa Fluor 568 channel [23]. Area fraction was calculated using the following equation: $AF = \frac{A_L}{A_L + A_D}$. Area live is determined by the number of pixels with a live signal in a spheroid, while area dead is based on the number of pixels with a spheroid. The data was analyzed using an LME model on JMP PRO 17 software to determine optimal media and seeding densities. The LME model considered factors like media and seeding density as full factorials, while the random effect accounted for the variations in passages performed across biological replicates.

2.3: Results

2.3.1: Morphology of A549 Spheroids

The optimization of both media and seeding density for A549 spheroids was examined through morphology and assay development to determine the best environment for growing 3D NSCLC cells. Morphology imaging was conducted for all underlying conditions; the images were captured on days 2, 4, and 6 in vitro. In examining spheroid development, it was found that media was not a significant factor in morphology, as F12k, DMEM, and RPMI exhibited similar morphological growth throughout the week. However, seeding density did show some observable morphological differences, as illustrated in **Figures 1-3**.

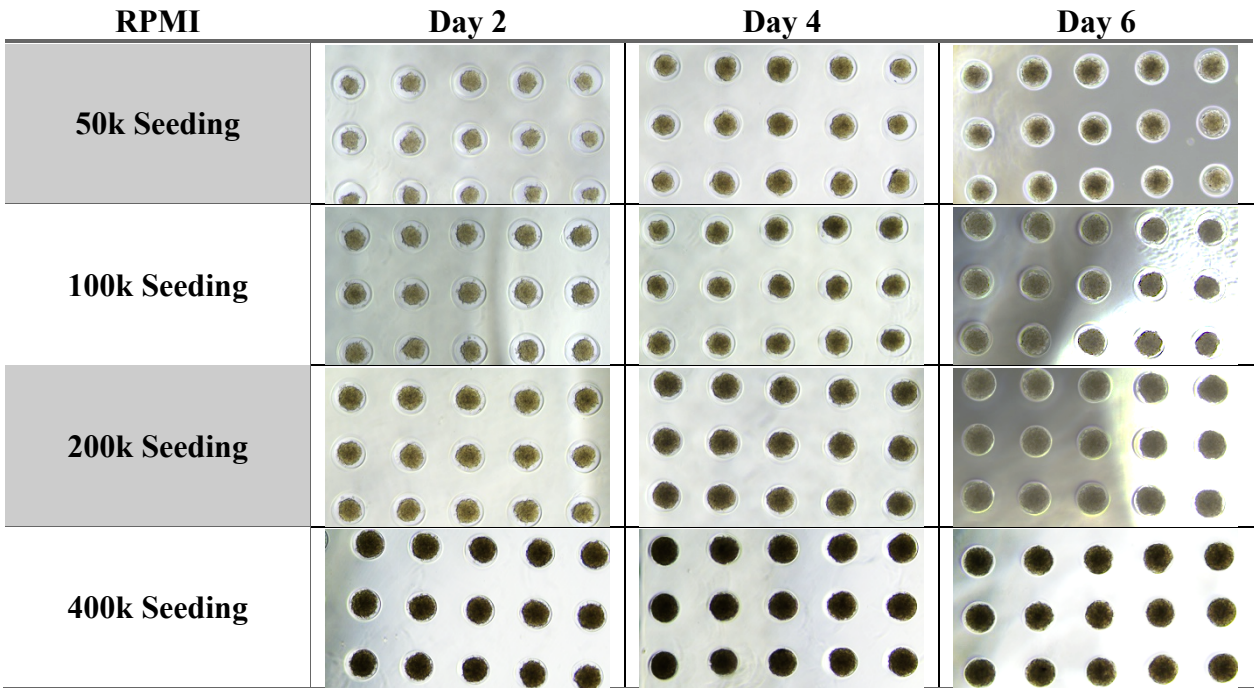

***Figure 1**: RPMI A549 spheroids at days in vitro (DIV) 2,4 and 6 at seeding densities 50 x10^3, 100 x 10^3, 200 x10^3, and 400 x 10^3.*

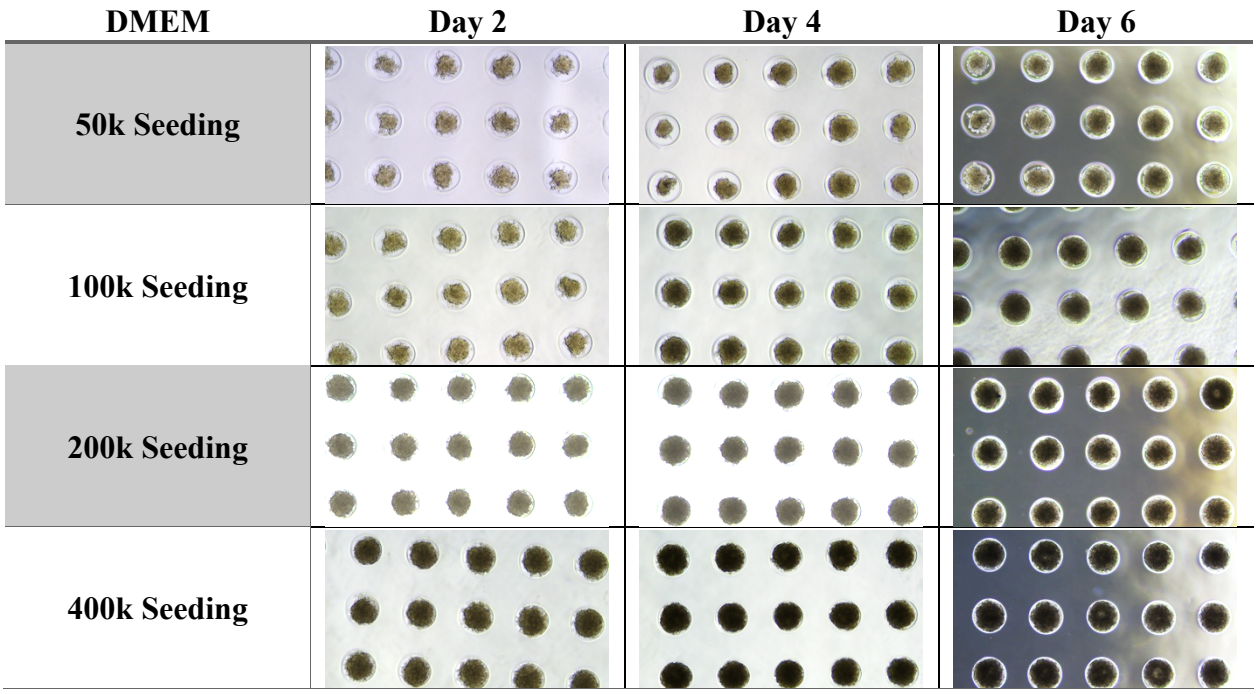

Figure 2: *DMEM A549 spheroids at days in vitro (DIV) 2,4 and 6 at seeding densities 50 x10^3, 100 x 10^3, 200 x10^3, and 400 x 10^3.*

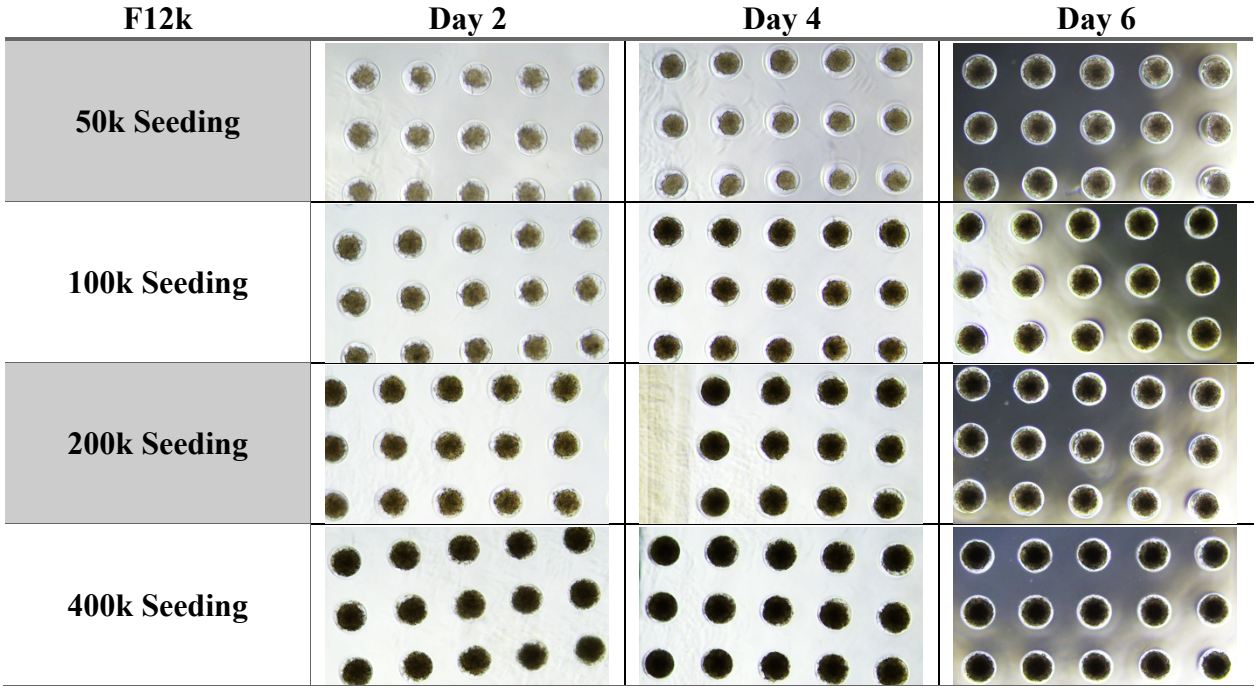

Figure 3: *F12k A549 spheroids at days in vitro (DIV) 2,4 and 6 at seeding densities 50 x10^3, 100 x 10^3, 200 x10^3, and 400 x 10^3.*

The morphological images of the A549 spheroids revealed new insights. Although the growth media displayed no noticeable differences, the seeding density did. Analyzing the morphological images of 200k and 400k seeding across all three media options reveals that by DIV 4, the spheroids have completely matured within their microtissue wells, presented in **Figures 1-3**. This overgrowth can result in various complications, especially cell death. Cells in the center consistently grow atop one another, limiting their access to essential nutrients from the media changes, leading to higher cell death rates. Compared to the 50k and 100k seeding densities, it is observed that by DIV 4, as shown in Figures 1-3, they have not entirely encapsulated in the microwell. This leads to more uniform cell growth and proliferation, making them very favorable for 7-day cell culture experiments.

2.3.2: ATP A549 Optimization

On day 7 in vitro, the ATP cell viability assay was performed on the microtissue gels with eight replicate spheroids gently removed for each conditional variable. The following operation was performed to normalize the ATP data: $\frac{ATP}{Pixel\ Area}$. The concentration of ATP is directly associated with a specific area defined as pixels or groups of pixels in an image that quantify ATP in cells [24]. The data were analyzed using the LME model with a Tukey HSD test, comparing the conditional variables side-by-side using the Least Square Means (LSM) model; p-value <0.0001 indicates the most significance, as seen in **Figures 4-7** and **Tables 1-4**.

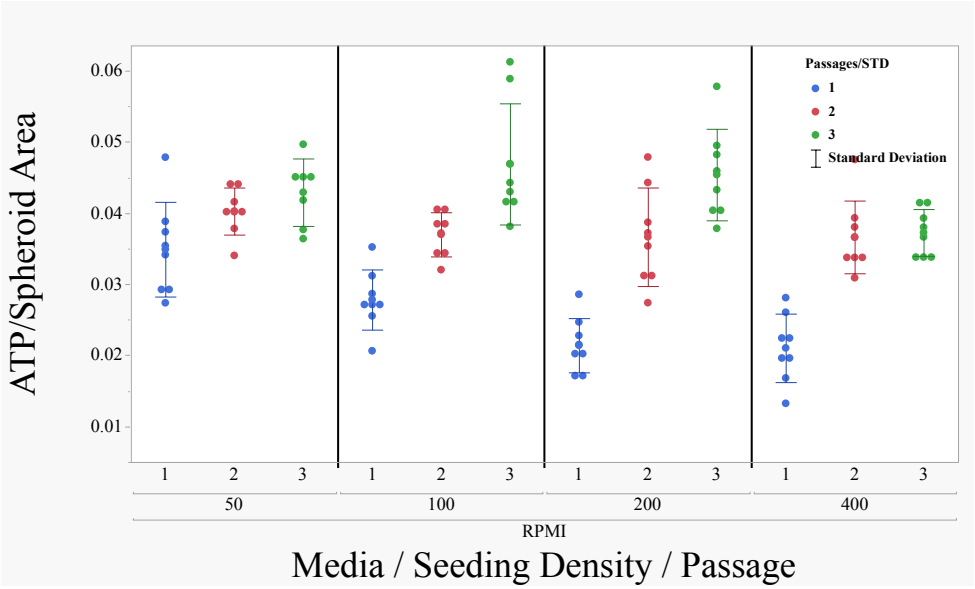

Figure 4*:Normalized RPMI ATP data across all seeding densities with three biological replicates from passages 1-3.*

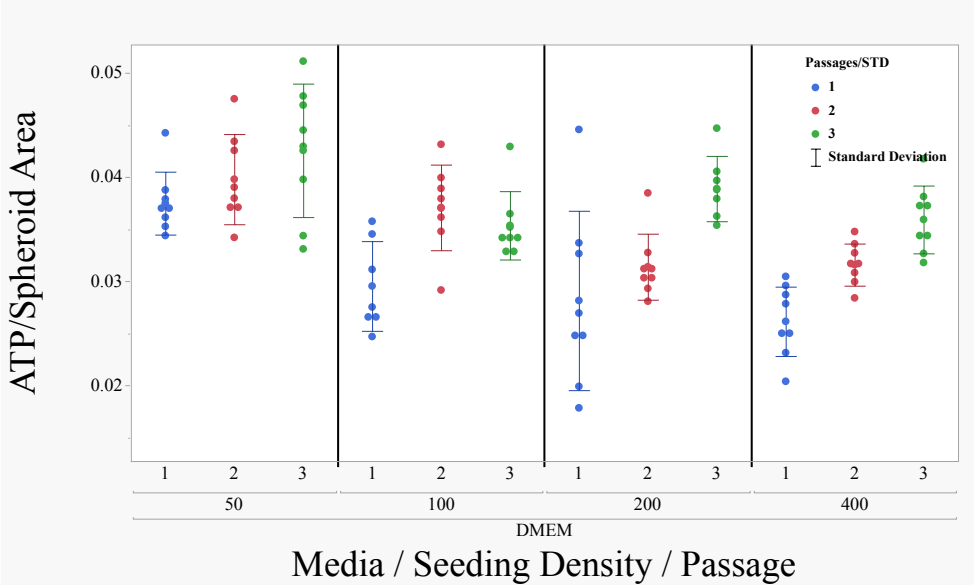

Figure 5*: Normalized ATP data in DMEM across all seeding densities with three biological replicates from passages 1-3.*

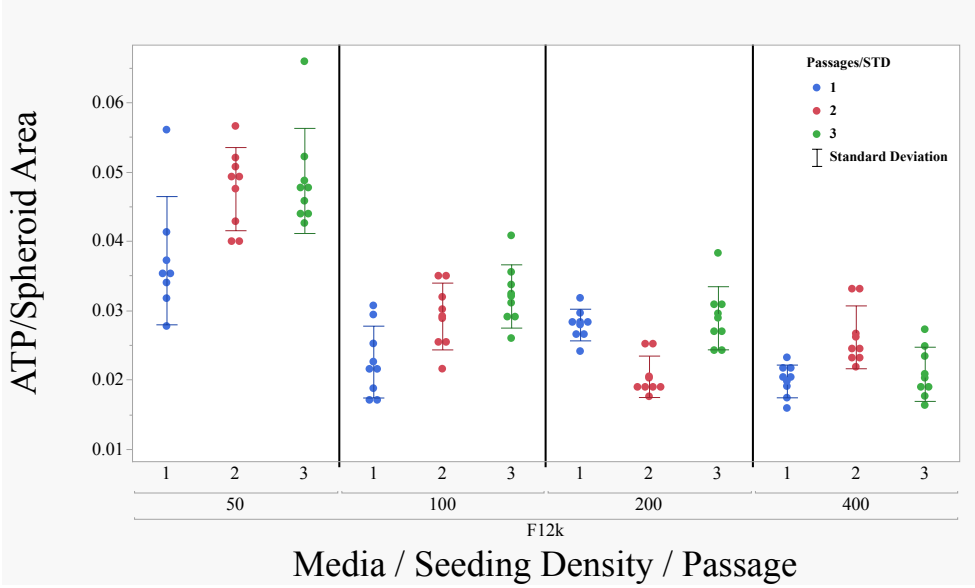

***Figure 6**: Normalized ATP data in F12k across all seeding densities with three biological replicates from passages 1-3.*

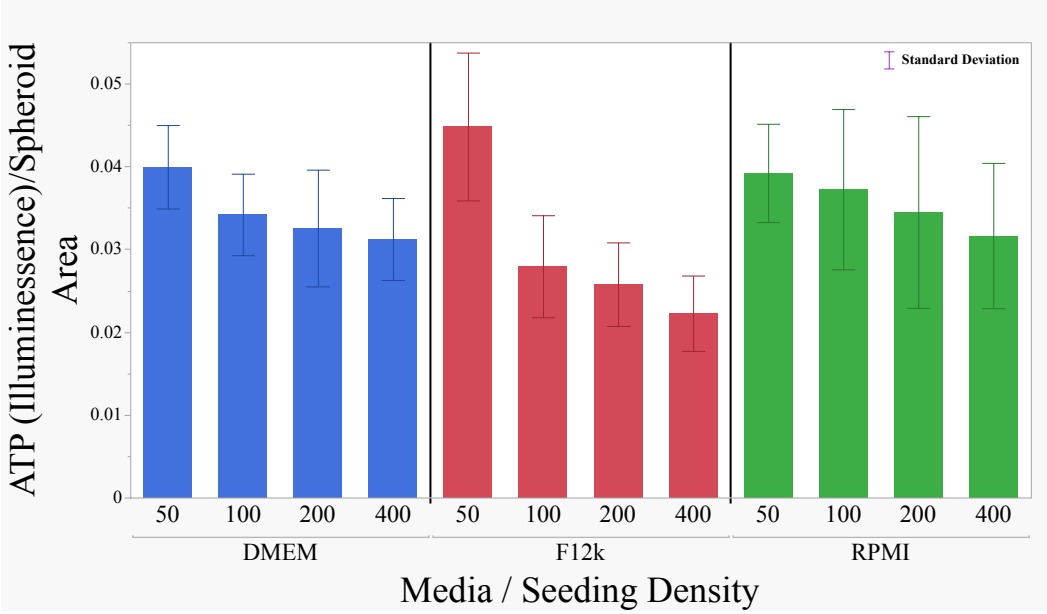

***Figure 7**: The graph presents normalized ATP data for all media and seeding density during optimization, compared side-by-side with the standard deviation illustrated by error bars.*

Media			Least Squares Means
RPMI	A		0.0357
DMEM	A		0.0345
F12k		B	0.0301

Table 1*: LME analysis with Tukey HSD test presents the LSM model for all pairwise comparisons among all media options. Letters with no connections indicate significance.*

Media	***-Media***	**Prob>|t|**
DMEM	***F12k***	<.0001*
DMEM	***RPMI***	0.3242
F12k	***RPMI***	<.0001*

Table 2*: The comparison of different media options can be visualized by the relative p-value obtained from side-by-side media evaluations.*

Seeding Density				Least Squares Means
50k	A			0.0413
100k		B		0.0330
200k		B		0.0310
400k			C	0.0283

Table 3*: LME analysis with Tukey HSD test presents the LSM model for all pairwise comparisons among all seeding density options. Those with non-connected letters showed significance.*

Seeding Density	***-Seeding Density***	**Prob>|t|**
50k	***100k***	<.0001*
50k	***200k***	<.0001*
50k	***400k***	<.0001*
100k	***200k***	0.1637
100k	***400k***	<.0001*
200k	***400k***	0.0393*

Table 4*: The comparison of different seeding densities can be visualized by the relative p-value obtained from side-by-side seeding evaluations.*

The pixel area of the spheroids was used to normalize the ATP data seen in **Figures 4-7**, which was then analyzed using the LME model. It was discovered that optimal growth media and seeding density existed. When comparing the media options side-by-side, a Tukey HSD test was conducted to evaluate all pairwise connections using an LMS model, as shown in **Table 1**. The results indicated that F12k performed worse, as demonstrated by the significant difference when compared to RPMI and DMEM. RPMI and DMEM were considered equally optimal, with no significant difference between them. The analysis of media options extends further with a significance table that displays the relative p-value for each media comparison. It was determined that F12k had a significance level of $p < 0.0001$ compared to RPMI and DMEM, as illustrated in **Table 2**. A similar comparison was carried out for DMEM and RPMI, but no significance was detected. Further testing is needed between DMEM and RPMI to determine the most optimal growth media.

The optimization of seeding density was analyzed using ATP data in a consistent format. Each of the four seeding densities underwent evaluation through all pairwise comparison Tukey HSD test, supported by an LMS model, as shown in **Table 3**. The table showed that by day 7, there was some level of significance between the seeding densities. There are three levels to the all-pairwise comparison. On its own, the 50k seeding showed the most promise, while the 100k and 200k options fell behind, and the 400k performed poorly in comparison. These points are further supported by the significance level when comparing the seeding densities head-to-head, represented by a p-value of $p < 0.0001$ being the most significant, as illustrated in **Table 4**. The comparison of 50k to all other seeding options showed significance, while 100k and 200k did not show significance to each other. A comparison of 100k and 400k revealed significance, whereas 200k and 400k also exhibited significant differences. The p-value for the 200k and 400k

comparison was not significant at < 0.0001, but the asterisk next to the values indicates there is significance between the two variables. The optimal seeding density for 7 days in vitro is 50k; additional testing will be conducted to compare 50k and 100k for 5 days in vitro. This experiment aims to determine whether a 50k seeding is optimal for day 5 experiments moving forward.

2.3.3: Live/Dead Analysis Media Optimization

Further analysis was required to optimize media and seeding density after examining the data from the ATP assay. A Live/Dead assay was conducted on day 5 in vitro, utilizing two replicates for each condition to ascertain the most optimal growth media and seeding density effectively. Live/Dead assay will consider the variables Intensity Fraction and Area Fraction. The analysis identified only one significant variable: Intensity fraction. Intensity fraction is calculated using the following formula: $IF = \frac{L_I}{L_I + D_I}$. The data were analyzed using the LME model with a Tukey HSD test, comparing the remaining media options and seeding density side-by-side, with a p-value <0.0001 indicating significance, as illustrated in **Figure 8** and **Tables 5 and 6**.

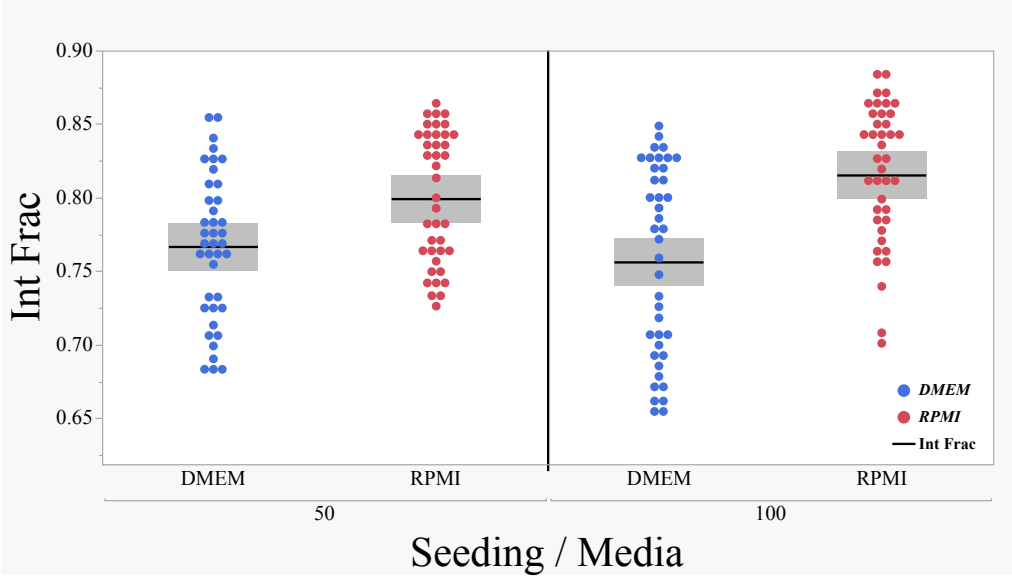

Figure 8*: Intensity fraction values displayed per condition; line of best fit was implemented to visualize the data points for side-by-side comparisons between conditions.*

Media	***Seeding Density***			**Least Squares Means**
RPMI	*100k*	A		0.815
RPMI	*50k*	A		0.799
DMEM	*50k*		B	0.766
DMRM	*100k*		B	0.756

Table 5*: LME analysis with Tukey HSD test presents the LSM model for all pairwise comparisons among all remaining conditions. Those with non-connected letters show significance. These comparisons were made based on the intensity fraction value.*

Media	***Seeding***	***-Media***	***-Seeding***	**Prob>|t|**
DMEM	***50***	***DMEM***	***100***	0.7956
DMEM	***50***	***RPMI***	***50***	0.0260*
DMEM	***50***	***RPMI***	***100***	0.0002*
DMEM	***100***	***RPMI***	***50***	0.0014*
DMEM	***100***	***RPMI***	***100***	<.0001*
RPMI	***50***	***RPMI***	***100***	0.4978

Table 6*: That significance can be visualized by the relative p-value based on the side-by-side media comparison with seeding density.*

Out of 20 segmented microtissue wells per condition, 10 were selected using MATLAB code for Live/Dead analysis. Intensity fraction was the only variable tested that showed any significance between media options, which was calculated using the following equation: $IF = \frac{L_I}{L_I + D_I}$. The intensity fraction data for both RPMI and DMEM is compared simultaneously in **Figure 8**. The data was analyzed using an LME model, and further comparison was performed between the two remaining media options. The pairwise comparison of Tukey HSD assessments was conducted using the LMS model for further support, as shown in **Table 5**. When evaluating

the media and seeding densities in this format, it is evident that RPMI at either 50k or 100k is the most optimal for A549 spheroid development. To further support this claim, **Table 6** displays the significant variance between each combination, with a p-value of $p < 0.0001$ being the most significant. In most cases, DMEM showed substantial differences from RPMI; although the p-values are not < 0.0001, they remain significant based on the asterisks next to the values. Seeding density showed no statistical difference between 50k and 100k, indicating they are the same on day 5 in vitro.

2.4 Discussion and Conclusion

2.4.1: Morphology of A549 Spheroids

3D cell culture was first developed in the early 1990s, incorporating extracellular substrates from in vivo cells into in vitro experimental models [25]. These 3D in vitro models have been used in various research in the field of biomedical sciences, especially in oncology research. When 3D cell culture models are used for drug testing, they show entirely different results compared 2D cell culture models due to their ability to have cell-cell interaction and extracellular matrix changes typically associated to in-vitro [25-28]. The A549 cell line has a well-researched history, but there is limited research focused explicitly on 3D/spheroid cell cultures. These challenges result from the cancer itself; the lung features many elongated narrow cavities where the tumor develops, creating an environment that presents multiple challenges and resulting in unique culture methods. A widely used 3D culture method known as hanging drop is popular for its cost-effectiveness and ability to produce cellular heterogeneity and hypoxic spheroids [29]. It also has limitations, such as differences in spheroid diameter, low throughput, and a reduction in oxygen and nutrients due to its non-microfluidic nature environment [30]. Many other methods also exist but come with cost and time limitations. Using 96-microtissue well molds establishes an optimal environment for spheroid growth and effectively demonstrates the typical intercellular and intracellular processes that can only be observed in vivo.

The primary objective of developing A549 3D cell cultures is to address the limitations inherent in conventional monolayer cell cultures, particularly regarding tumor cell heterogeneity and tissue architecture [31]. Many factors contribute to maximizing the growth of these NSCLC spheroid models. Growth media is crucial in providing cells with the necessary nutrients for their development and maintenance. Some cell types might need certain non-

essential amino acids to assist in these cellular processes more effectively. [32]. Accurately determining the optimal seeding density is essential, as overseeding and under-seeding can adversely affect experimental outcomes if the cells do not receive adequate growth conditions. This is illustrated in the article by Yildiz-Ozturk et al., who utilized the same molds but tested a broader range of seeding densities. Their seeding densities of 5x10 ^5 and 1x10^6 became overgrown and deemed unsuitable for future experimentation [21].

2.4.2: ATP Analysis of A549 Spheroids

The ATP assay was performed on day 7 in vitro. This viability assay is commonly used due to its ability to estimate the number of viable cells in High Throughput Screenings (HTS). When cells lose their membrane integrity, their ability to synthesize ATP through metabolism diminishes, leading to the depletion of remaining ATP in the cytoplasm [33]. ATP assay is a versatile and straightforward assessment that can provide insight into a cell's inner membrane environment. The greater the amount of ATP a cell produces, the more it is typically linked to a larger number of living cells, indicating the viability and proliferation of the cell.

When optimizing cell culture, it is essential to produce viable cells that exhibit a strong rate of proliferation and viability. Cell proliferation is a crucial indicator for understanding the inner biological processes, including genes, proteins, and pathways, and how they influence the overall survival and death of a cell [34]. All cells within the human body, whether healthy or cancerous, rely on specific proteins to promote growth and vitality, resulting in prolonged cell viability. Each growth medium has its own properties of nutrients, gelling agents, and other essential components that foster cell growth. Every organism has optimal growth requirements, which is also true for living cell culture models. Improved growth can result in enhanced models, leading to more successful experimental outcomes benefiting patients. Evaluating the A549

spheroids using the ATP viability assay is crucial for understanding their proliferation potential and identifying the media and seeding requirements that yield the best results.

2.4.3: Live/Dead Assay Optimization of A549 Spheroids

The ATP assay assessed the viability and proliferation of the A549 spheroids under various media and seeding density options. RPMI and DMEM showed no significant differences in their ATP analysis, indicating that the metabolic viability of the spheroids is statistically the same. Further testing is required to identify the optimal growth media for A549 spheroids. The Live/Dead assay assessment will determine the number of live and dead cells present within individual spheroids. Live cells will be stained green using Calcein-AM, a pro-fluorescent marker. This marker is commonly used to assess cytotoxicity because live cells upregulate it. The cytoplasmic esterase activity in live cells removes the AM group, forming fluorescent Calcein within those cells [35]. Dead cells are stained red by Ethidium homodimer, a viability stain with a high affinity for nucleic acids compared to other dyes, which aids its ability to not require a washing step, unlike Propidium Iodide [36].

The Live/Dead assay will provide additional insights into cell viability. We know that media options like DMEM and RPMI supply sufficient nutrients for cell proliferation. However, we need to determine how many of these cells are alive and emitting ATP signals. Spheroids are unlike typical 2D cell cultures; they form a rod within the microtissue wells being constructed as a culmination of multiple cells. A spheroid itself will emit signs of viability and proliferation, but examining the individual cells that make up the spheroid is just as important. Optimizing the overall development of A549 spheroids involves troubleshooting and examining every aspect of the spheroids to ensure the best results.

2.4.4: Conclusion

To sum up, based on the data collected through morphological imaging and assay assessment of both ATP and Live/Dead, the most optimal growth media and seeding density for A549 spheroid development can be determined. According to the data from both ATP and Live/Dead, RPMI 1640 is the optimal media for A549 3D culture. The seeding density optimization for A549 spheroids was 50k, determined through morphology and ATP assay and further validated by a Live/Dead assay. In aim 2, A549 spheroids will be cultured in RPMI at a seeding density of 50k for drug testing analysis.

Chapter 3: Aim 2: Testing Chemosensitivity of A549 Spheroids using Viability Assay Imaging

3.1: Introduction

The FPM approach involves administering drugs directly to patient-derived tumor cells to generate insights for personalized therapeutic guidance [37]. This strategy is being implemented in the drug testing of the A549 NSCLC spheroids developed in Aim 1. A drug test aims to evaluate the overall presence or absence of specific drugs or their metabolites in a biological sample [38]. Many drugs aim to treat many variants of NSCLC; the three that will be of focus are Cisplatin, Sotorasib, and Afatinib. Cisplatin is considered a first-line therapy, usually given alone or in combination with another therapy, also referred to as Platinum-based combination therapy. Sotorasib and Afatinib belong to the same drug family, as they are both targeted therapies. Targeted therapies in cancer treatment are drugs that target specific proteins causing cancer to proliferate and grow [39].

Cisplatin, a platinum-based therapy, causes cells to enter cell death through apoptosis. Apoptosis occurs when cisplatin covalently binds to amino acids, resulting in DNA strand breaking and triggering apoptotic cell death [40]. A study by Mohiduddin et al. concluded that monotherapy with Cisplatin is more effective at targeting KRAS-dependent A549 cells than combined with pemetrexed or pemetrexed alone [41]. Sotorasib is a targeted therapy for the KRAS G12C mutation. The KRAS mutation occurs in A549 cells, specifically G12S variant. Although it differs slightly, the aim is to determine whether the serine substitution produces a similar therapeutic effect as the cysteine change. Sotorasib binds to the KRAS mutation, keeping the cysteine protein inactive, inhibiting signaling pathways associated with cellular growth proliferation. [42]. Afatinib is a targeted therapy directed at the EGFR mutation and is

considered a second-line treatment for advanced squamous cell carcinoma. Afatinib works by inversely inhibiting Epidermal Growth Factor Receptor (EGFR), which plays a crucial role in tumor cell proliferation [43]. A549 cells are commonly used in EGFR research and are typically regarded as wildtype in these studies, indicating that Afatinib is expected to have a minimal effect on A549 cells.

3.2: Methods & Materials

3.2.1: Cell Culture & Microtissue Formation

Human NSCLC alveolar epithelial cancer cells (A549; ATCC) were cultivated in the optimal media identified from our findings in aim 1: Roswell Park Memorial Institute 1640 Medium (A1049101; Gibco^{TM}). RPMI was supplemented with 10% Fetal Bovine Serum (S11150; GeminiBio) and 1% of 10,000 IU/mL penicillin/10,000 µg/ml streptomycin (ICN1670249; Fisher-Scientific), then incubated in a 5% CO_2 environment at 37°C. To form spheroids, we used the previously stated conditions; a seeding density of 50 x 10^3 was deemed most optimal through data analysis for a 7-day drug testing experiment.

3.2.2: A549 Spheroid Drug Dosing

Five days after seeding into gels, A549 microtissues were treated with various drugs: 3181.81 µM of Cisplatin (Sigma-Aldrich, 1003757368), 35,000 µM of Sotarasib (Sigma-Aldrich, SRR00089), and 35,000 µM of Afatanib (Sigma-Aldrich, SML3109). 25 mg of Cisplatin was dissolved in saline (NaCl, Sigma-Aldrich; 15230162, Gibco^{TM}) to obtain a stock concentration of 3181.81 µM. 5 mg of Sotorasib and 10 mg of Afatanib were dissolved in Dimethyl Sulfoxide (MT-25950CQC, Corning) to obtain a stock concentration of 35,000 µM for both. The stock solution provided a concentration of 35 µM, while the lower final concentrations of 0.7 and 7 µM were diluted from this stock. The control group, however, used saline/DMSO and media without dilution from the stock solution. The concentration levels were increased from the original 0.5, 5, and 25 µM due to the displacement within the gels, which accounts for the 1.4x increase in dosage. Each drug and dosing condition is represented by 2 microtissue replicates in a 24-well plate. After dosing, the A549 microtissues were placed back into the incubator at 5% CO_2 at 37°C for 72 hours. Phase contrast images were captured using a Leica

DMi1 Inverted Phase Contrast Microscope, both prior to dosage and after a 72-hour exposure to the drugs, to assess any morphological changes in the cells.

3.2.3: CellTiter-Glo Cell Viability Assay: Drug Testing

Microtissue gels were removed from the 24-well plate and placed into 35 mm Petri dishes with 3-4 mL of specified media. Spheroids were rinsed from the gels using media. After isolation, they were transferred to a 96-well plate with 90 µL of media, and the tip was shortened to prevent damaging the cells. Imaging was performed for the spheroid in each well to assess its pixel area, which served as a basis for normalizing the ATP results. A multi-channel pipette was used to add 90 µL of room-temperature ATP assay reagent (CellTiter-Glo, Promega) to each well. The plates were moved to a plate rocker for 5 minutes at 150 RPM and left at room temperature for 25 minutes. Finally, the plates were placed in a microplate reader (Synergy HTX, BioTek) to measure the luminescence of the spheroids with the ATP reagent.

3.2.4: Statistical Analysis

The CellTiter-Glo Assay involved eight microtissue replicates per condition over three weeks. The ATP data for A549 cells was standardized based on the cross-sectional area. The operation used to normalize ATP by the pixel area of the spheroids was: $\frac{ATP}{Pixel\ Area}$. After normalizing the data, an LME model with full factorial of drug and dosage with a randosme effect of passage (week) was executed using JMP PRO 17 software (Cary, NC). This analysis enabled a side-by-side comparison of all the drugs and their dosage ranges, making it easier to identify all the drug effects for Cisplatin, Sotorasib, and Afatinib regarding cell viability and proliferation.

3.3 Results

3.3.1 Drug Testing A549 Spheroids Using ATP Assay

The ATP assay was performed on day 7, following a 72-hour exposure period. On day 5, Cisplatin, Sotorasib, and Afatinib were dosed to the spheroids at dosage ranges of 0.7, 7, and 35 µM, and the control group at zero µM. Morphology of the microtissue molds was taken pre-dosage and post-dosage for the three drugs at each of the dosages before ATP assessment, shown in **Figures 9-11**. The spheroids were carefully removed from the microtissue molds, with eight replicate spheroids collected for each drug and dosage. During this stage, it was found that Afatinib at 35 µM could not undergo ATP testing due to the complete disintegration of all spheroids after being removed from the mold, as illustrated in **Figure 12**. The ATP data was normalized using the operation: $\frac{ATP}{Pixel\ Area}$. The ATP, pixel area, and normalized ATP data were graphed in **Figures 13-15,** and further analysis was performed using an LME model. Least Square Means (LSM) plots were implemented to thoroughly examine the drug effect of Cisplatin, Sotorasib, and Afatinib simultaneously for drug and dosage for ATP, Pixel Area and Normalized ATP data, as shown in **Figures 16-18.**

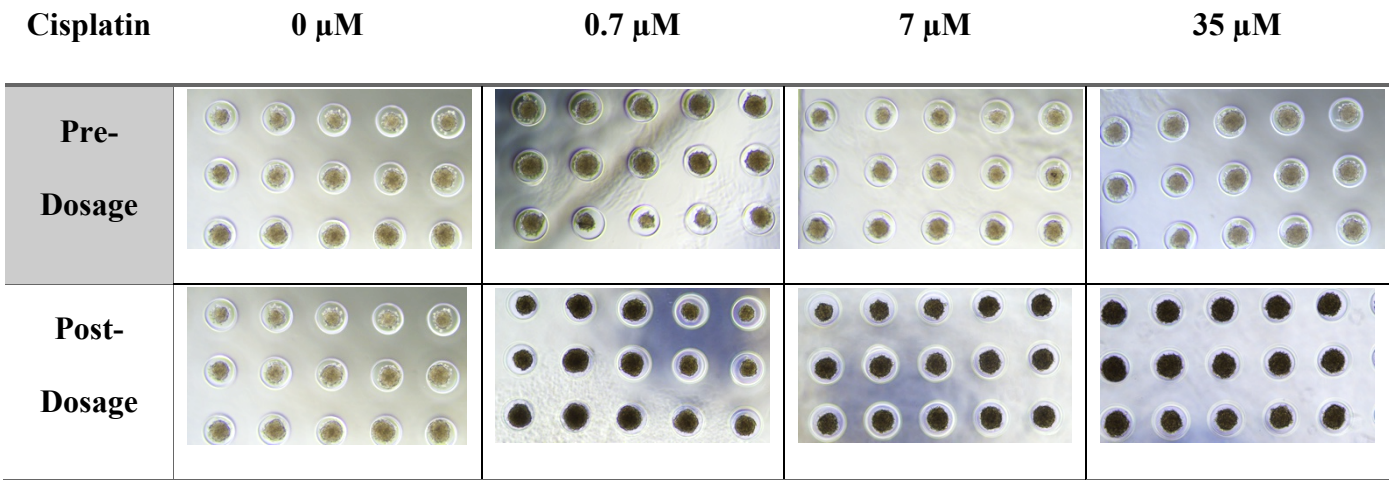

Figure 9*: Morphology images pre- (DIV 5) and post-dosage (DIV 7) of 0, 0.7, 7 and 35 µM of Cisplatin.*

Sotorasib	0 µM	0.7 µM	7 µM	35 µM
Pre-Dosage	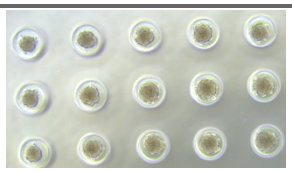	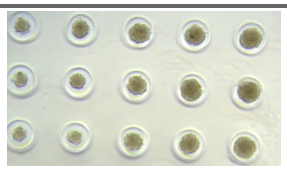	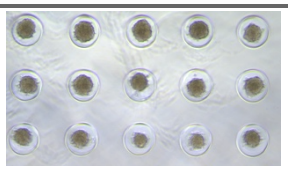	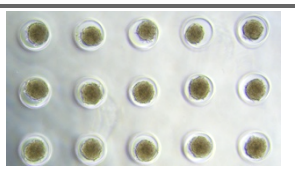
Post-Dosage	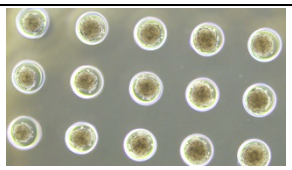	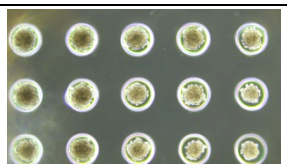	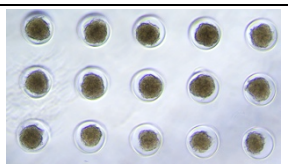	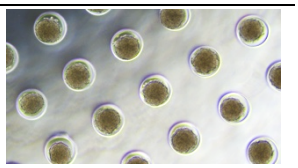

***Figure 10**: Morphology images pre- (DIV 5) and post-dosage (DIV 7) of 0, 0.7, 7 and 35 µM of Sotorasib.*

Afatinib	0 µM	0.7 µM	7 µM	35 µM
Pre-Dosage	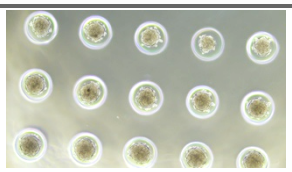	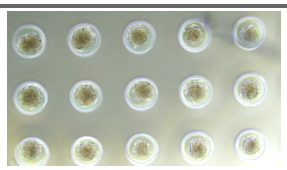	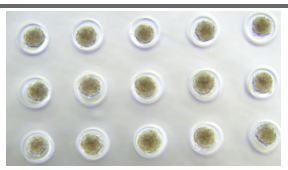	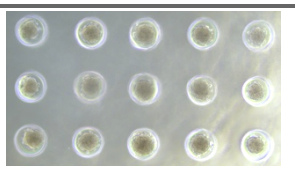
Post-Dosage	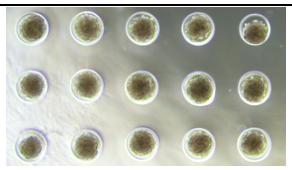	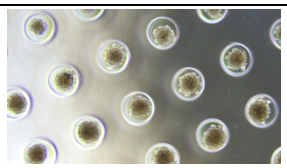	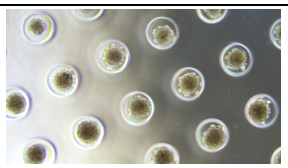	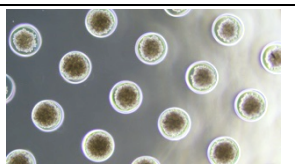

***Figure 11**: Morphology images pre- (DIV 5) and post-dosage (DIV 7) of 0, 0.7, 7 and 35 µM of Afatinib.*

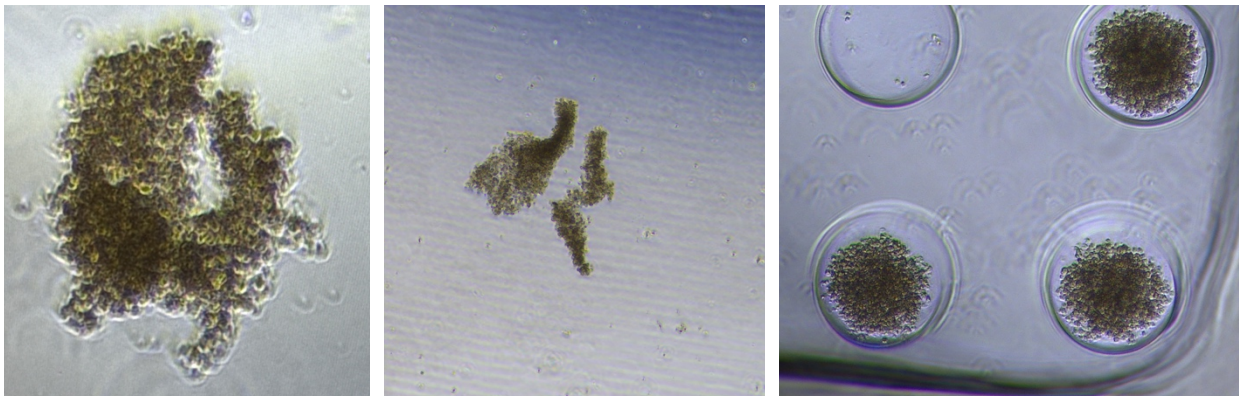

***Figure 12**: Examples of spheroid morphologies disrupted by high-dose drug administration.*

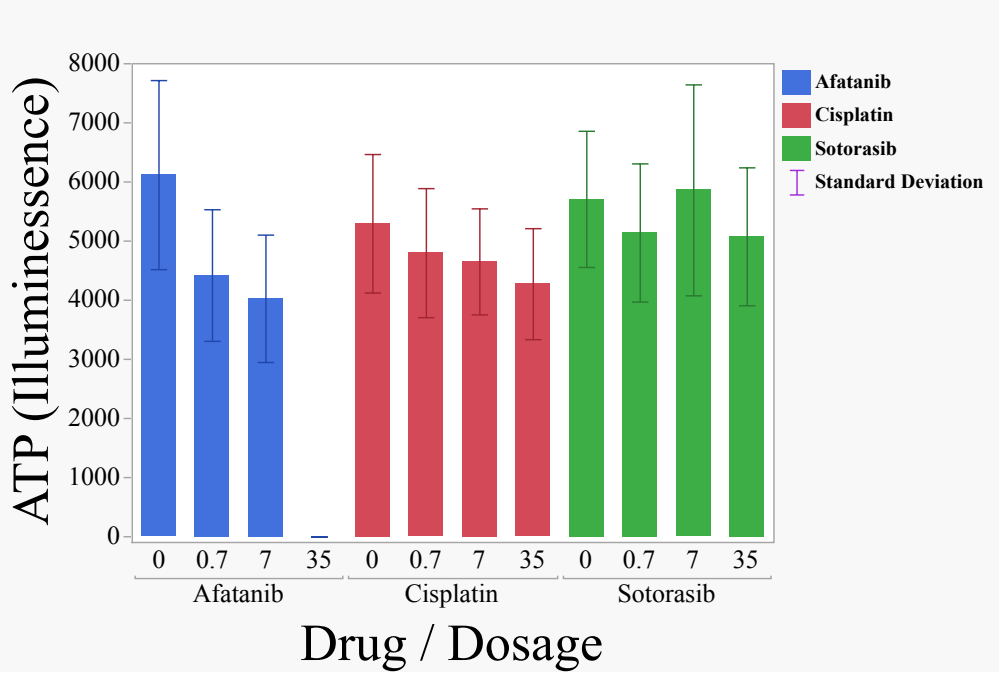

***Figure 13**: ATP data results for all drugs (Afatinib, Cisplatin, & Sotorasib) at each dosage (0 µM, 0.7 µM, 7 µM and 35 µM) compared side-by-side with standard deviation parameters included by the error bars. 35 µM could not be included for Afatinib due to the lack of any ATP.*

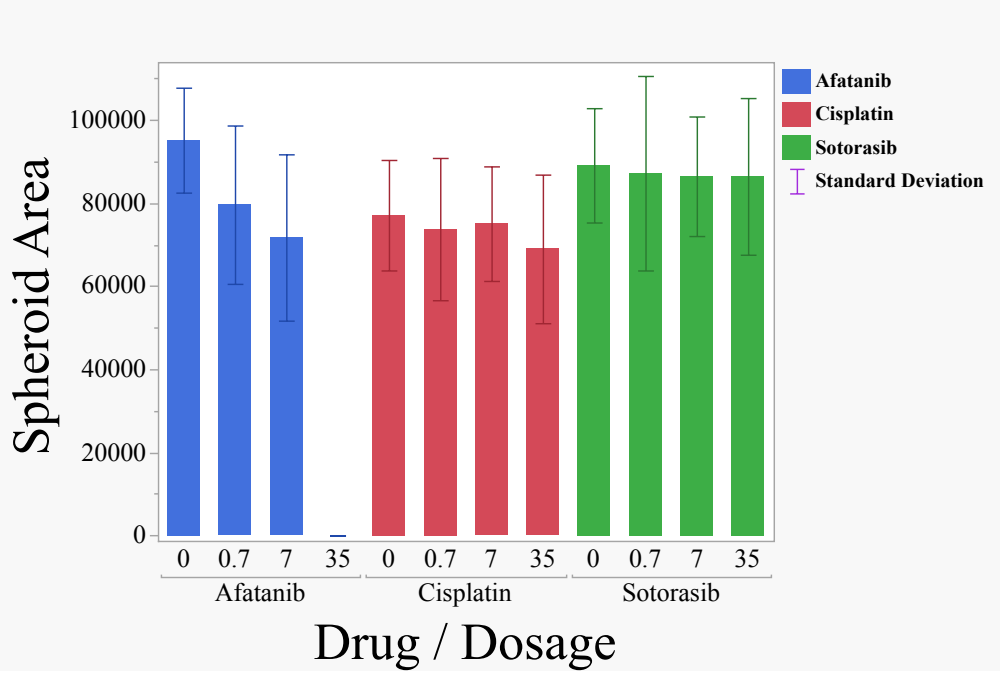

***Figure 14**: Pixel Area data results for all drugs (Afatinib, Cisplatin, & Sotorasib) at each dosage (0 µM, 0.7 µM, 7 and 35 µM) compared side-by-side with standard deviation parameters included by the error bars. 35 µM could not be included for Afatinib due to the lack of viable spheroids for the pixel area analysis, skewing the results.*

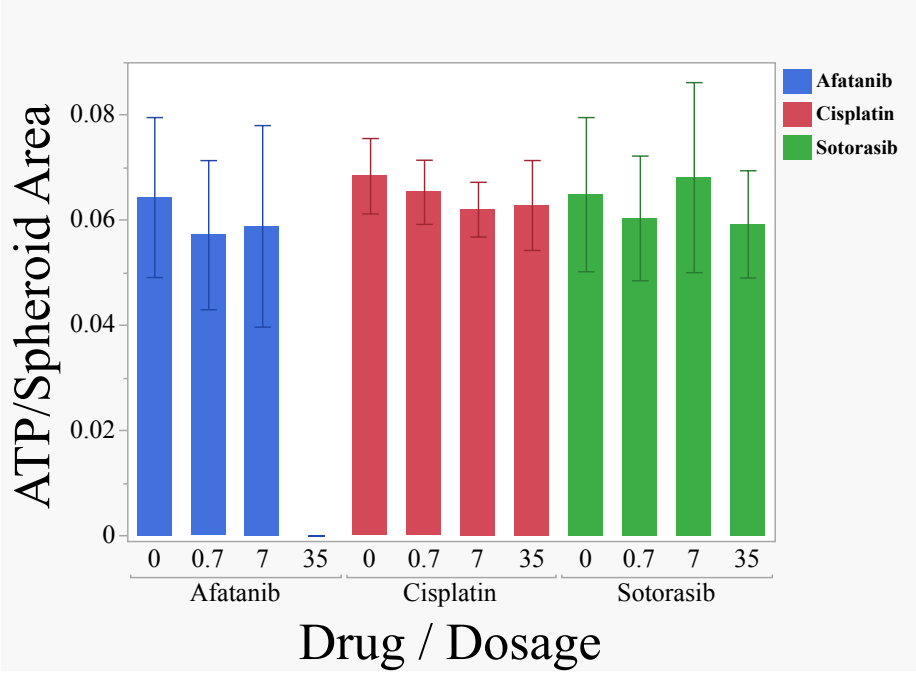

***Figure 15**: Normalized ATP data results for all drugs (Afatinib, Cisplatin, & Sotorasib) at each dosage (0 µM, 0.7 µM, 7 µM and 35 µM) compared side-by-side with standard deviation parameters included by error bars. 35 µM could not be included for Afatinib due to the lack of any ATP/Pexel Area values for that dosage because of spheroids disintegration, skewing the results.*

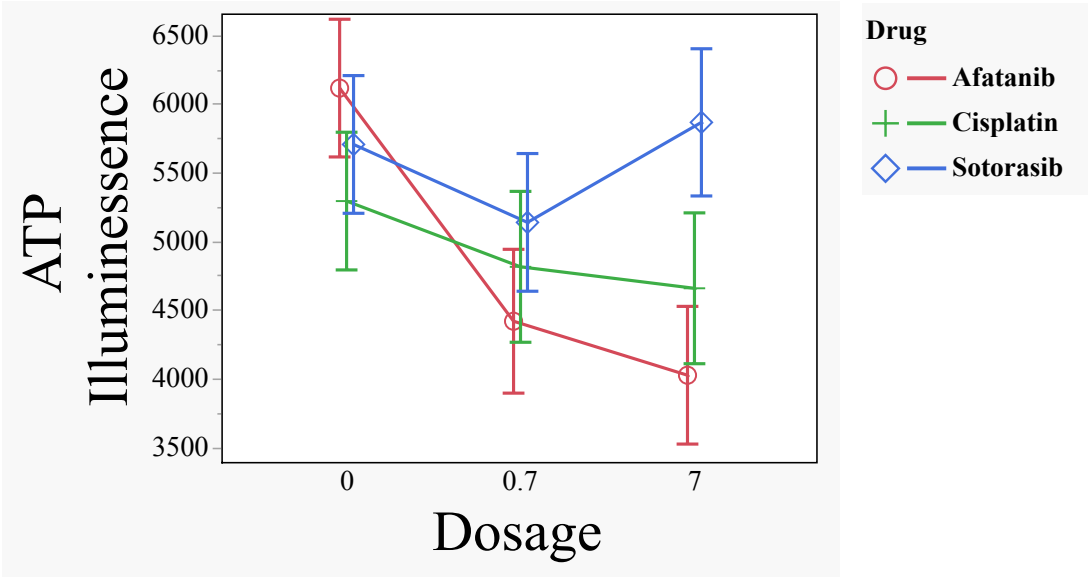

***Figure 16**: LSM plot of ATP data for all drugs (Afatinib, Cisplatin, and Sotorasib) with each dosage (0 µM, 0.7 µM, 7 µM) compared simultaneously. The 35 µM dosage could not be included because Afatinib has no ATP values for that level due to the disintegration of spheroids, skewing the results. Confidence limits are illustrated with the addition of error bars.*

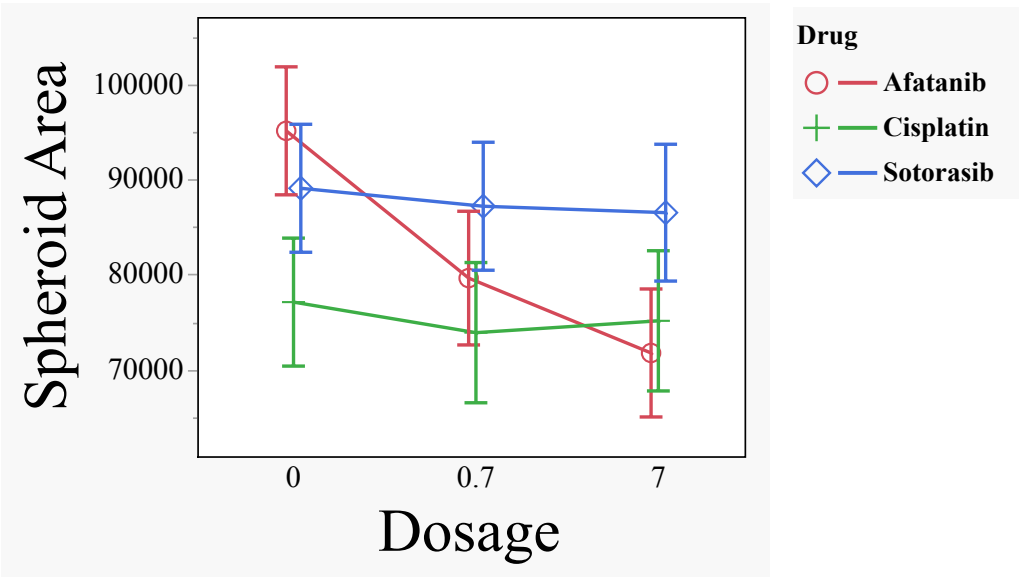

Figure 17: *LSM plot of Pixel Area data for all drugs (Afatinib, Cisplatin, and Sotorasib) with each dosage (0 µM, 0.7 µM, 7 µM) compared simultaneously. The 35 µM dosage could not be included because Afatinib does not have spheroids for Pixel Area analysis due to disintegration, skewing the results. Confidence limits are illustrated with the addition of error bars.*

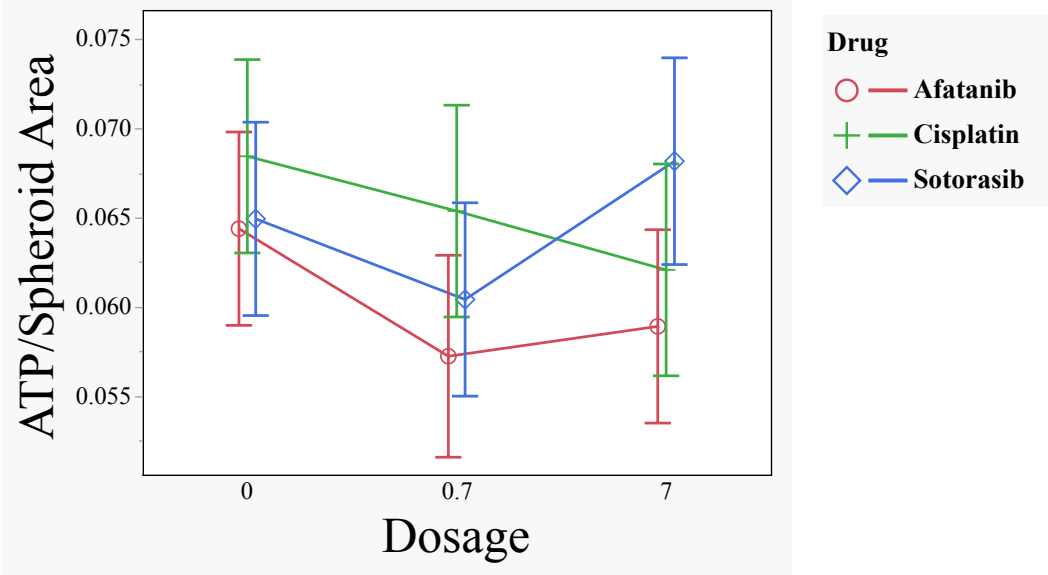

Figure 18*: LSM plot of Normalized ATP data for all drugs (Afatinib, Cisplatin, and Sotorasib) with each dosage (0 µM, 0.7 µM, 7 µM) compared simultaneously. The 35 µM dosage could not be included because Afatinib does not have spheroids for ATP/Pixel Area analysis due to disintegration, skewing the results. Confidence limits are illustrated with the addition of error bars.*

The morphology of the cells was assessed both before and after administering the three drugs (Cisplatin, Sotorasib, and Afatinib). Inside the microtissue wells, there were no observable differences following the 72-hour exposure period, as evidenced by the images in **Figures 9-11**. Once ATP analysis was conducted, it was found that after gently removing the spheroids administered with Afatinib at 35 µM from the microtissue molds, they could not maintain their spheroid shape and completely dissociated, as illustrated in **Figure 12**. The complete

disintegration of the A549 spheroids renders ATP analysis for Afatinib at 35 µM impossible, resulting in a value of 0 for all data. ATP assay was performed for the remaining conditions without any issues.

ATP data was normalized using the pixel area of the individual spheroids using the following operation: $\frac{ATP}{Pixel\ Area}$. It is common practice to normalize ATP data because certain cell-based features influence the oxygen consumption rate, which directly affects the results. Nevertheless, the normalized data from this experiment may have concealed the overall impact of the drugs. Raw ATP and pixel area are included in the analysis. The data collected from ATP, pixel area, and normalized ATP were all graphed individually, comparing the drugs and the dosages simultaneously, along with standard deviation error bars, as seen in **Figures 13-15**. ATP and pixel area graphs are included to demonstrate the drug effect trend that normalized ATP data cannot assess. The complete breakdown of spheroids at 35 µM Afatinib prevented data collection, thus excluding this concentration from all data sets in the drug effect comparison study. When comparing the drugs side-by-side, it is evident that both ATP and pixel area indicate a drug effect for Afatinib, as demonstrated by the decrease in the overall trend line for ATP and pixel area. This same effect was not seen in Cisplatin or Sotorasib, as shown in the LMS plot in **Figures 16 & 17.** ATP analysis indicates that Afatinib is affecting both the proliferation and viability of the A549 cells, as seen in the change from 0 µM to 7 µM. Conversely, Cisplatin and Sotorasib may be demonstrating the ability to slow or stop the growth of A549 spheroids, yet additional testing is required to confirm these findings. After normalizing the data, as shown in the LMS plot in **Figure 18**, it was found that no drug exhibited any statistically relevant drug effect for the A549 spheroids. This potentially means that ATP per

pixel area is considerably normal, indicating that for the size of the spheroids, the amount of ATP produced is proportional for each of the three dosages.

3.4: Discussion and Conclusion

3.4.1: Drug Testing Analysis for NSCLC Spheroids

ATP analysis assessed cell proliferation and viability changes after dosing the A549 spheroids with drugs (Cisplatin, Sotorasib, and Afatinib) at concentrations of 0.7, 7, and 35 μM. A decrease in viable cells can lead to two primary outcomes: the inhibition of cell metabolism and/or proliferation or cell death [44]. Afatinib had significant changes to viability and proliferation, as seen by the individual analysis of ATP and pixel area data. This outcome was unexpected because A549 cells are wildtype to Afatinib drug, yet they exhibited the most potent drug effect in the ATP assay. The mechanism of action for Afatinib is that it inhibits EGFR mutation in the cell, which is a major contributor to tumor cell proliferation [43]. The gene copy number of EGFR in A549 cells is estimated to be approximately 2.8, further supporting this data. [45]. Additional analysis is essential to thoroughly comprehend the extent to which EGFR influences the proliferation and growth of A549 cells.

Even though Sotorasib targets the KRAS mutation, the difference between the cysteine and serine substitutions is too significant, and the drug does not provide the same effect observed by ATP analysis. The inhibition resulting from Sotorasib's mechanism of action is expected to disrupt signals related to cell growth and proliferation, which should be observable in the ATP assay. In the study by Barrios-Bernal et al., they discuss a combination therapy of Sotorasib with Metformin, which exhibited promising results for cytotoxicity and apoptosis of the G12S KRAS mutation [46]. Sotorasib alone does not show the same effects on A549 G12S KRAS mutated cells as seen with the combination therapy; further analysis is needed to substantiate this assertion. Cisplatin, like Sotorasib, demonstrated a nonsignificant drug effect on the A549 spheroids. Cisplatin is a chemotherapy used in many cancer treatments due to its high

potency to destroy both tumor cells and health cells through apoptotic cell death. Overall, ATP analysis proved it did not affect A549 spheroids. Baek et al. explain that the A549 spheroid's diameter remains unchanged until reaching a dosage threshold of approximately 50 μM [47]. In our drug testing comparison study, we did not surpass a dosage of 35 μM. Therefore, further analysis with higher dosages may be necessary to confirm this data.

3.4.2: Conclusion

In short, ATP analysis provided preliminary insight into the drug effect of A549 spheroids using the drugs (Cisplatin, Sotorasib, and Afatinib). Even though Afatinib displayed drug effect, it could only be evident under unnormalized data conditions. Although widely used, the ATP assay may not be the most effective measure of proliferation for specific drugs, as seen in the ATP LME graphs in the study by Zein-Sabatto et al. [48]. Factors such as higher dosages may need to be evaluated for Sotorasib and Cisplatin to assess any significant ATP effect. Further testing with ATP can still be conducted to better understand whether the halting or slowing of proliferation by Sotorasib and Cisplatin is accurate by reducing the exposure time of the drugs to 24 and 48 hours.

3.4.3: Future Work

Further analysis must be conducted with ATP data before proceeding to future experiments. The use of Optical Coherence Tomography for drug testing analysis of A549 spheroids as a Functional Precision Medicine approach still needs to be performed in the future.

References

1. *Lung cancer guide: What you need to know*. Guide | What You Need to Know | American Cancer Society. (n.d.). https://www.cancer.org/cancer/types/lung-cancer.html
2. Siegel, R. L., Kratzer, T. B., Giaquinto, A. N., Sung, H., & Jemal, A. (2025). Cancer statistics, 2025. *CA: A Cancer Journal for Clinicians*, *75*(1), 10–45. https://doi.org/10.3322/caac.21871
3. *Difference Small Cell & Non-small cell lung cancer*. moffitt. (n.d.). https://www.moffitt.org/cancers/lung-cancer/faqs/what-is-the-difference-between-small-cell-lung-cancer-non-small-cell-lung-cancer/
4. Schabath, M. B., & Cote, M. L. (2019). Cancer progress and priorities: Lung Cancer. *Cancer Epidemiology, Biomarkers & Prevention*, *28*(10), 1563–1579. https://doi.org/10.1158/1055-9965.epi-19-0221
5. Nooreldeen, R., & Bach, H. (2021). Current and future development in lung cancer diagnosis. *International Journal of Molecular Sciences*, *22*(16), 8661. https://doi.org/10.3390/ijms22168661
6. Minna, J. D., Roth, J. A., & Gazdar, A. F. (2002). Focus on lung cancer. *CellPress*, *1*(1), 49–52. https://doi.org/10.1016/S1535-6108(02)00027-2
7. Vidaver, R. M., Shershneva, M. B., Hetzel, S. J., Holden, T. R., & Campbell, T. C. (2016). Typical time to treatment of patients with lung cancer in a multisite, US-based study. *Journal of Oncology Practice*, *12*(6). https://doi.org/10.1200/jop.2015.009605
8. Muslim, Z., Stroever, S., Razi, S. S., Poulikidis, K., Baig, M. Z., Connery, C. P., & Bhora, F. Y. (2023). Increasing time-to-treatment for lung cancer: Are we going backward? *The Annals of Thoracic Surgery*, *115*(1), 192–199. https://doi.org/10.1016/j.athoracsur.2022.06.016
9. Yang, H.-T., Shah, R. H., Tegay, D., & Onel, K. (2019). Precision oncology: Lessons learned and challenges for the future. *Cancer Management and Research*, *Volume 11*, 7525–7536. https://doi.org/10.2147/cmar.s201326
10. Longo, D. L. (2012). Tumor heterogeneity and Personalized Medicine. *New England Journal of Medicine*, *366*(10), 956–957. https://doi.org/10.1056/nejme1200656
11. Letai, A., Bhola, P., & Welm, A. L. (2022). Functional precision oncology: Testing tumors with drugs to identify vulnerabilities and novel combinations. *Cancer Cell*, *40*(1), 26–35. https://doi.org/10.1016/j.ccell.2021.12.004
12. Sheng, S., Margarida Bernardo, M., Dzinic, S. H., Chen, K., Heath, E. I., & Sakr, W. A. (2018). Tackling tumor heterogeneity and phenotypic plasticity in cancer precision medicine: Our experience and a literature review. *Cancer and Metastasis Reviews*, *37*(4), 655–663. https://doi.org/10.1007/s10555-018-9767-4
13. Jia, D., Jolly, M. K., Kulkarni, P., & Levine, H. (2017). Phenotypic plasticity and cell fate decisions in cancer: Insights from Dynamical Systems theory. *Cancers*, *9*(7), 70. https://doi.org/10.3390/cancers9070070
14. Panovska, D., & De Smet, F. (2022). Functional precision oncology: The next frontier to improve glioblastoma outcome? *International Journal of Molecular Sciences*, *23*(15), 8637. https://doi.org/10.3390/ijms23158637
15. Yang, H., Zhang, N., & Liu, Y.-C. (2020). An organoids Biobank for recapitulating tumor heterogeneity and personalized medicine. *Chinese Journal of Cancer Research*, *32*(3), 408–413. https://doi.org/10.21147/j.issn.1000-9604.2020.03.12

16. Liu, C. J., Smith, J. T., Wang, Y., Ouellette, J. N., Rogers, J. D., Oliner, J. D., Szulczewski, M., Wait, E., Brown, W., Wax, A., Eliceiri, K. W., & Rafter, J. (2024). Assessing cell viability with dynamic optical coherence microscopy. *Biomedical Optics Express*, *15*(3), 1408. https://doi.org/10.1364/boe.509835
17. Aumann, S., Donner, S., Fischer, J., & Müller, F. (2019). Optical Coherence Tomography (OCT): Principle and technical realization. *High Resolution Imaging in Microscopy and Ophthalmology*, 59–85. https://doi.org/10.1007/978-3-030-16638-0_3
18. Jung, Y., Klein, O. J., Wang, H., & Evans, C. L. (2016). Longitudinal, label-free, quantitative tracking of cell death and viability in a 3D tumor model with OCT. *Scientific Reports*, *6*(1). https://doi.org/10.1038/srep27017
19. Sundararajan, R., Salameh, T., Camarillo, I. G., Prabu, R. R., Natarajan, A., & Sankaranarayanan, K. (2014). Irreversible electroporation: A drug-free cancer treatment. *Electroporation-Based Therapies for Cancer*, 219–243. https://doi.org/10.1533/9781908818294.219
20. Arodin Selenius, L., Wallenberg Lundgren, M., Jawad, R., Danielsson, O., & Björnstedt, M. (2019). The cell culture medium affects growth, phenotype expression and the response to selenium cytotoxicity in A549 and Hepg2 Cells. *Antioxidants*, *8*(5), 130. https://doi.org/10.3390/antiox8050130
21. Yildiz-Ozturk, E., Saglam-Metiner, P., & Yesil-Celiktas, O. (2021). Lung carcinoma spheroids embedded in a microfluidic platform. *Cytotechnology*, *73*(3), 457–471.https://doi.org/10.1007/s10616-021-00470-7
22. *Animal Cell Culture Guide | ATCC*. ATCC Animal Cell Culture Guide. (n.d.). https://www.atcc.org/resources/culture-guides/animal-cell-culture-guide
23. Zein-Sabatto, A., St. Angelo, K., Madnick, S. J., Hoffman-Kim, D., Morgan, J. R., & Lee, J. (2025). Multi-assay assessment of cytotoxicity reveals multiple mechanisms of action in 3D microtissues. *Scientific Reports*, *15*(1). https://doi.org/10.1038/s41598-025-86792-4
24. Cacciamali, A., Villa, R., & Dotti, S. (2022). 3d Cell cultures: Evolution of an ancient tool for new applications. *Frontiers in Physiology*, *13*. https://doi.org/10.3389/fphys.2022.836480
25. Lee, S.-Y., Koo, I.-S., Hwang, H. J., & Lee, D. W. (2023). In vitro three-dimensional (3D) cell culture tools for spheroid and organoid models. *SLAS Discovery*, *28*(4), 119–137. https://doi.org/10.1016/j.slasd.2023.03.006
26. Wong, H.-L., Wang, M.-X., Cheung, P.-T., Yao, K.-M., & Chan, B. P. (2007). A 3D collagen microsphere culture system for GDNF-secreting HEK293 cells with enhanced protein productivity. *Biomaterials*, *28*(35), 5369–5380. https://doi.org/10.1016/j.biomaterials.2007.08.016
27. Gurski, L. A., Petrelli, N. J., Jia, X., & Farach-Carson, M. C. (2010). 3D matrices for anti-cancer drug testing and development. *Oncology Issues*, *25*(1), 20–25. https://doi.org/10.1080/10463356.2010.11883480
28. Huang, G.-S., Tseng, T.-C., Dai, N.-T., Fu, K.-Y., Dai, L.-G., & Hsu, S. (2015). Fast isolation and expansion of multipotent cells from adipose tissue based on Chitosan-selected primary culture. *Biomaterials*, *65*, 154–162. https://doi.org/10.1016/j.biomaterials.2015.07.003
29. Rasouli, M., Safari, F., Kanani, M.H., Ahvati, H. (2024). Principles of Hanging Drop Method (Spheroid Formation) in Cell Culture. In: Turksen, K. (eds) Autophagy in

Development and Disease. Methods in Molecular Biology, vol 2879. Humana, New York, NY. https://doi.org/10.1007/7651_2024_527
30. Białkowska, K., Komorowski, P., Bryszewska, M., & Miłowska, K. (2020). Spheroids as a type of three-dimensional cell cultures—examples of methods of preparation and the most important application. *International Journal of Molecular Sciences*, *21*(17), 6225. https://doi.org/10.3390/ijms21176225
31. Suzuki, R., Hotta, K., & Oka, K. (2015). Spatiotemporal quantification of subcellular ATP levels in a single Hela cell during changes in morphology. *Scientific Reports*, *5*(1). https://doi.org/10.1038/srep16874
32. Weiskirchen, S., Schröder, S. K., Buhl, E. M., & Weiskirchen, R. (2023). A beginner's Guide to Cell Culture: Practical Advice for preventing needless problems. *Cells*, *12*(5), 682. https://doi.org/10.3390/cells12050682
33. Riss TL, Moravec RA, Niles AL, et al. Cell Viability Assays. 2013 May 1 [Updated 2016 Jul 1]. In: Markossian S, Grossman A, Arkin M, et al., editors. Assay Guidance Manual [Internet]. Bethesda (MD): Eli Lilly & Company and the National Center for Advancing Translational Sciences; 2004-. Available from: https://www.ncbi.nlm.nih.gov/books/NBK144065/
34. Riss T, Niles A, Moravec R, et al. Cytotoxicity Assays: In Vitro Methods to Measure Dead Cells. 2019 May 1. In: Markossian S, Grossman A, Arkin M, et al., editors. Assay Guidance Manual [Internet]. Bethesda (MD): Eli Lilly & Company and the National Center for Advancing Translational Sciences; 2004-. Available from: https://www.ncbi.nlm.nih.gov/books/NBK540958/
35. Adan, A., Kiraz, Y., & Baran, Y. (2016). Cell proliferation and cytotoxicity assays. *Current Pharmaceutical Biotechnology*, *17*(14), 1213–1221. https://doi.org/10.2174/1389201017666160808160513
36. Haugland, R. P., MacCoubrey, I. C. & Moore, P. L. Dual-fluorescence cell viability assay using ethidium homodimer and calcein AM. Google Patents (1994).
37. Letai, A., Bhola, P., & Welm, A. L. (2022). Functional precision oncology: Testing tumors with drugs to identify vulnerabilities and novel combinations. *Cancer Cell*, *40*(1), 26–35. https://doi.org/10.1016/j.ccell.2021.12.004
38. McNeil SE, Chen RJ, Cogburn M. Drug Testing. [Updated 2023 Jul 29]. In: StatPearls [Internet]. Treasure Island (FL): StatPearls Publishing; 2025 Jan-. Available from: https://www.ncbi.nlm.nih.gov/books/NBK459334/
39. *Targeted therapy for cancer*. Targeted Therapy for Cancer - NCI. (n.d.). https://www.cancer.gov/about-cancer/treatment/types/targeted-therapies#what-is-targeted-therapy
40. Gold JM, Raja A. Cisplatin. [Updated 2023 May 22]. In: StatPearls [Internet]. Treasure Island (FL): StatPearls Publishing; 2025 Jan-. Available from: https://www.ncbi.nlm.nih.gov/books/NBK547695/
41. MOHIUDDIN, M., & KASAHARA, K. (2021). Cisplatin and pemetrexed have distinctive growth-inhibitory effects in monotherapy and combination therapy on*kras*-dependent A549 lung cancer cells. *Cancer Genomics - Proteomics*, *18*(4), 579–590. https://doi.org/10.21873/cgp.20282
42. Jaber, N. (2021, June 21). *Sotorasib is first KRAS inhibitor approved by FDA*. Sotorasib is First KRAS Inhibitor Approved by FDA - NCI. https://www.cancer.gov/news-events/cancer-currents-blog/2021/fda-sotorasib-lung-cancer-kras

43. Moosavi L, Preuss CV, Polineni R. Afatinib. [Updated 2024 Feb 28]. In: StatPearls [Internet]. Treasure Island (FL): StatPearls Publishing; 2025 Jan-. Available from: https://www.ncbi.nlm.nih.gov/books/NBK542248/
44. Sazonova, E. V., Chesnokov, M. S., Zhivotovsky, B., & Kopeina, G. S. (2022). Drug toxicity assessment: Cell proliferation versus cell death. *Cell Death Discovery*, *8*(1). https://doi.org/10.1038/s41420-022-01207-x
45. Suzawa, K., Toyooka, S., Sakaguchi, M., Morita, M., Yamamoto, H., Tomida, S., Ohtsuka, T., Watanabe, M., Hashida, S., Maki, Y., Soh, J., Asano, H., Tsukuda, K., & Miyoshi, S. (2015). Antitumor effect of afatinib, as a human epidermal growth factor receptor 2-targeted therapy, in lung cancers harboring oncogene alterations. *Cancer Science*, *107*(1), 45–52. https://doi.org/10.1111/cas.12845
46. Barrios-Bernal, P., Lucio-Lozada, J., Ramos-Ramírez, M., Hernández-Pedro, N., & Arrieta, O. (2023). A novel combination of Sotorasib and metformin enhances cytotoxicity and apoptosis in kras-mutated non-small cell lung cancer cell lines through MAPK and P70S6K inhibition. *International Journal of Molecular Sciences*, *24*(5), 4331. https://doi.org/10.3390/ijms24054331
47. An, S. S., Seo, O. W., Lee, J., Hulme, J., & Baek, N. (2016). Real-time monitoring of Cisplatin cytotoxicity on three-dimensional spheroid tumor cells. *Drug Design, Development and Therapy*, *Volume 10*, 2155–2165. https://doi.org/10.2147/dddt.s108004
48. Zein-Sabatto, A., St. Angelo, K., Madnick, S. J., Hoffman-Kim, D., Morgan, J. R., & Lee, J. (2025a). Multi-assay assessment of cytotoxicity reveals multiple mechanisms of action in 3D microtissues. *Scientific Reports*, *15*(1). https://doi.org/10.1038/s41598-025-86792-4